FEM for Wind Flow on Abstracted Urban Structures

Giada Risso, Stephan Simonis, Jun Zhang

Stockholm May 24, 2017

Project work for DD2365:
Advanced Computation in Fluid Mechanics.
Johan Hoffman, Van Dang Nguyen, Johan Jansson, Niclas Jansson
Kungliga Tekniska Högskolan

Contents

1 Abstract

The term *urban canyon* ideally refers to a relatively narrow street with buildings lined up continuously along both sides. In the real world, a broader definition of the term has been applied, including urban streets that are not necessarily flanked by buildings continuously on both sides, thus allowing gaps on the bounding walls of the canyon. An important determinant of characteristic airflow regimes observed within urban canyons is the geometry [1]. Particularly interesting is how it influences the transition between flows. Many cases of these effects can be categorized in terms of a threshold $\frac{W}{H}$, where W denotes the street width and H the building height. The assessment made within this report is focused on the air flow structure between two buildings. The main goal was to create a valid wind flow model within this simplified setting and evaluate it for various ratios. A Finite Element solver was used to obtain a transient solution for the abstracted flow field. The achieved results demonstrate the significance of ratio changes and therefor highlight the importance of numerical simulations in urban planning.

2 Introduction

A majority of the global population currently lives and works in urban areas. This urbanization is expected to increase and has recently inspired many urban-centered studies. The wind flows within cities, especially the local turbulence levels, directly affect pedestrian mobility and comfort [2]. Precisely these flow structures, although on a larger scale, represent the wind environment within which new buildings are to be placed and which is essential for both, provision of clean air and construction aspects.

In urban planning, it is crucial to model the wind flow. It is generally accepted that the relative height (H), width (W) and length (L) of a canyon are the most important factors for the resulting flow regime [3]. For this reason, we begin with the construction of a simplified two-dimensional model that focuses on the height and the width ratio.

As a validation of the following model we compared our results with the study provided by Kovar-Panskus [1], where a detailed comparison between numerical simulations and wind tunnel experiments is given. Our simulation has been performed to examine the variation with a stream-wise aspect ratio width/height of the mean flow patterns in a street canyon consisting of two buildings. The cases $\frac{W}{H} = 1$, 0.3 and 2 are provided.

Studying the vortex generation between two buildings that have two different heights is another possible application of this model. Moreover, we have investigated the influence of a third obstacle placed between the buildings. Considering different simple geometries, the main intention is to give a significant example that shows how the wind flow changes in this case not just looking at the velocity vectors but also at the pressure.

3 Equation and Simplifications

The Navier-Stokes equations (NSE) were used to model the flow field. They comprise several conservation forms, namely continuity and momentum. In particular we assume a single-phased, incompressible and Newtonian flow such that the equation can be written in the following way:

$$\text{(NSE):} \quad \begin{cases} \dot{u} + (u \cdot \nabla)\, u + \nabla p - \nu \Delta u = f \\ \nabla \cdot u = 0 \end{cases} \tag{1}$$

At this point, it is notable that considering previous literature, we decided to set the kinematic viscosity ν equal to $2.9 \cdot 10^{-3}$ and the source function f equal to zero, which excludes gravity effects. Our domain consists of a cut-out volume with a constant velocity entering from one lateral side – perpendicular to it. We consider the side opposite to the inlet as the outlet where we applied a zero-pressure boundary condition. Finally, "slip" boundary conditions ($u \cdot n = 0$) were added on the building surfaces, the ground and the top of the domain. Further description is given below.

4 2D Model and Method

On the two-dimensional nature of the flow, we consider the vertical cross-sections at mid-canyon level. The models with the ratios $\frac{W}{H} = 1$, 0.3 and 2 represent two rectangular buildings of equal height $H = 20[m]$ and distance $W = 20[m]$, $6[m]$ or $40[m]$ in between. The inlet velocity has been set as constant $u_{in} = 8[\frac{m}{s}]$ with its direction parallel to the ground coming from the left side of the domain in all our simulations. These definitions add up to a Reynolds number of approximately $\mathrm{Re} = 1.84 \cdot 10^4$. We set the right side of the domain as the zero-pressure outlet and finally consider slip boundary conditions on the remaining parts of the domain boundary (floor, ground and upon the buildings).

For a better visualization of the vortex evolvement we perform an initial refinement of the mesh in the area between the buildings where we expect vortices to appear. We refine the zone from the ground up to the height of $25[m]$, which is $5[m]$ above the building height. Above this region, the main flow is vortex free such that our choices are reasonable. In further sections we will refer to the domain for $\frac{W}{H} = 1$ as standard model. A plot of the refined mesh in this case can be found in Figure 1 below. Including the individual building width of $5[m]$, the total size of the volume is $40[m] \times 30[m]$. We chose this cut-out section to keep the computational time reasonable as well as to focus on the flow in between the buildings.

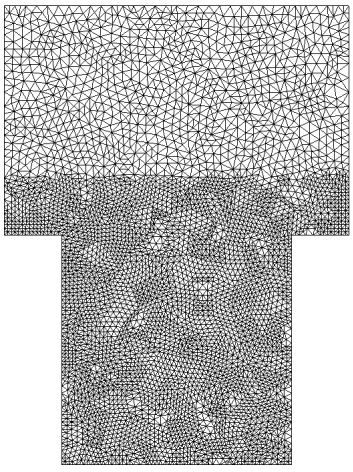

Figure 1: Refined initial mesh for the 2D with $W/H = 1$.

The numerical solution of equation 1 is constructed with a Finite Element method (FEM). As a computational platform we used the *FEniCS* environment to implement the weak residual form. A transient solution was obtained by applying the Midpoint method. For the setting above we fixed the stability parameter to $\delta = 0.1 \cdot h$ where h denotes the minimum cell size within the refined mesh. To fulfill the CFL-condition, the time step size was set to $\Delta t = 0.02$.

The overall time interval for the computations was limited to $t \in [0, 10]$, where t is measured in seconds.

5 Results

In summary, we conducted tests for

- $\frac{W}{H} = 1$: $W = 20[m]$, $H = 20[m]$
- $\frac{W}{H} = 0.3$: $W = 6[m]$, $H = 20[m]$
- $\frac{W}{H} = 2$: $W = 40[m]$, $H = 20[m]$
- $\frac{W}{H} = 1$: $W = 20[m]$, $H_1 = 25[m]$ and $H_2 = 15[m]$
- $\frac{W}{H} = 1$: $W = 20[m]$, $H_1 = 15[m]$ and $H_2 = 25[m]$
- $\frac{W}{H} = 1$ with an additional obstacle in between,

where H_1 denotes the height of the building on the left side of the domain and H_2 the height of the second one. The associated solution plots, contained in the figures mentioned below can be found in the Appendix.

5.1 Varying distance-height ratio

We start with illustrating the differences of the main vortex at the change of $\frac{W}{H}$. As mentioned before, we consider three different cases. In order to compare each solution to the results found in [4] we compute the average velocity field and visualize the corresponding streamlines. To get an overview of the magnitude and directions within the air flow of the standard model, its vector field is plotted at the change of time. Figures 3, 4, 5, 6 and 7 show the velocity vectors respectively for the times $t = 0.02$, 2.5, 5.0, 7.5 and 10.0 seconds. The streamlines of the average velocity field (computed from $t = 1$ to $t = 10$) are plotted in Figure 8b. We compare this to Figure 8a, which is the experimental result taken from [4]: Kim et al. (1999). In the same manner, Figures 9 and 10 show the results for a validation of the cases $\frac{W}{H} = 0.3$ and $\frac{W}{H} = 2$, respectively.

5.2 Different geometries

Varying individual building heights

Changing the relative heights of the two buildings gives the possibility of making more observations. In order to retain the Reynolds number of the standard model, we choose the height of the first building (in the left of the domain) H_1 and of the second one (on the right) (H_2) such that they satisfy the propriety:

$$\frac{H_1 + H_2}{2} = H = 20[m]. \tag{2}$$

Figure 11 shows the averaged flow streamlines (from $t = 1$ to $t = 10$) of the two opposite cases $H_1 > H_2$ and $H_1 < H_2$.

Adding an obstacle between the buildings

The final analysis that we will provide is about adding a third building of height $10[m]$ and width $5[m]$ in the middle of our standard geometry. In Figure 2 the streamlines of the averaged velocity vectors are plotted. We observe that more vortices are generated than in the standard geometry. Additionally, to get a better view on the directions of the individual movements, the velocity average vector field is visualized in Figure 12. Moreover, detailed streamline plots at several time steps are provided in Figure 18.

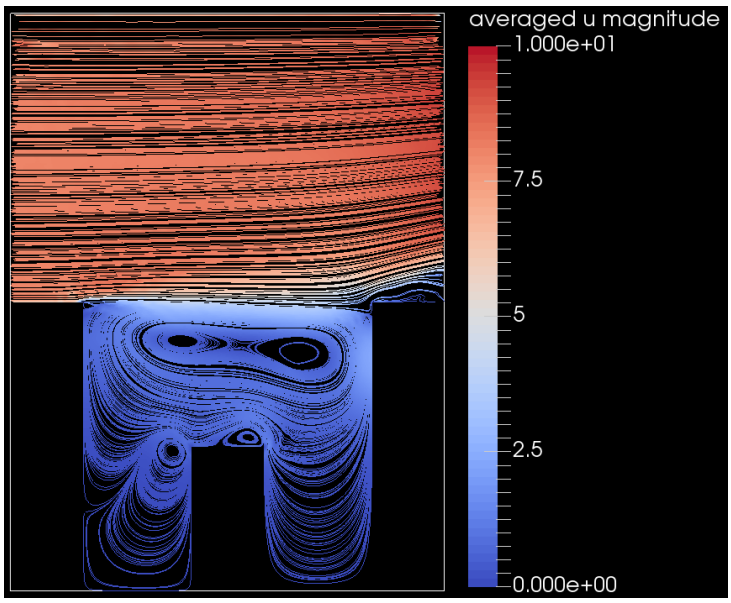

Figure 2: Streamline plot of averaged velocity field

Figure 13, which represents the pressure norm average from $t = 1$ to $t = 10$, gives rise to the impression that the pressure norm is very low in every region of the domain. Comparing this to Figure 15 we can observe that the average is not a valid approximation of the pressure. Additionally, we should not take its norm into further account. Instead we will continue with Figure 15, which visualizes the pressure at the change of time for $t = 2$, $t = 4$, $t = 6$ and $t = 8$ seconds. For a more complete study, we also attached the corresponding pressure value for the standard geometry in Figure 14. Note that the latter two cited figures use the same color grid for plotting the results in order to make the comparison easier.

6 Conclusion

After validating the results for several width-height ratios it is important to point out that taking only the velocity average into account is not very convenient, since it is and will be just an average. One reason for this loss of information is the, with W increasing, time the vortex needs to develop within the canyon. In general, we observed that the evolution as well as the position of the main vortex seem to change periodically. Figure 17 visualizes this center change of the largest appearing vortex for the standard geometry. Despite the unpredictable nature of the appearing vortexes one may conclude that after a long enough time period the structure will reach its initial position or, from a different point of view, will build up again. Averaging the solution over this time interval should then lead to a vortex, which is centered more or less

in the middle of the canyon.

Nevertheless, the comparison of the averaged solution with the experimental results of [4] was useful in terms of validation for the first three test cases, where we came to the conclusion that the vector field directions agree. Furthermore, the differences to [4] show that in a real life application, a transient numerical solution over a sufficiently long time interval should be more reliable, since surface forces and air mixing (resulting from the vortex development) are variable in time and thus an averaged solution may lead to incorrect conclusions.

Moreover, looking at a study provided by Tim R. Oke in 1988 [5], which illustrates a non-experimental investigation of the flow regimes at the change of the width-height ratio $\frac{W}{H}$, we can conclude that our model simulates the overall vortex shape as expected. To be more specific, an excerpt of Oke's analysis [5] is given in Figure 16. Note that in [5] the ratio between height and width is defined as $\frac{H}{W}$. The flow of $\frac{W}{H} = 2$ behaves as wake interference flow whilst the flows of $\frac{W}{H} = 1$ and $\frac{W}{H} = 0.2$ are skimming flows.

Moving to another configuration with different heights enables us to investigate the vortex developing close to the second building. In case of $H_1 > H_2$, see Figure 11a, we notice that another vortex is generated close to the second building. The first building creates a wind shade for the smaller second one, which leads to the additional vortex appearing. The case $H_1 < H_2$ exposes the second building to the main flow, such that the surface force induced by the wind flow should be highly increased.

As we expected, adding the third obstacle is strongly affecting the solution. We can see in Figure 2 that the main vortex in the top part in the middle is still present, although new structures are generated near to the obstacle. The velocity vector field directions are similar to the standard case, where the flow regime around the main vortex was mainly moving clockwise. What this all amounts to is that the upper part of the obstacle in between is exposed to a manifold of vortexes. This effect could be useful for further studies, for example pollutant transport. Due to the focus on the generic air flow model in this report, we will leave these applications open and proceed with the conclusion.

Since an examination of the streamlines is not sufficient for a complete study, the pressure at the change of time may be useful for further analysis. As we can see in Figure 14 and 15 the pressure region generated around the main vortex is similar, whereas in the three buildings case, new pressure differences are generated around the structure in the middle. From a comparison of the pressure average to the velocity average we conclude that the averaged pressure is not a reliable result to look at, since the vortices and their pressure fields are located in different regions.

As a last point we recapitulate our approach for this report. A two-dimensional section model of the above defined urban canyon was implemented with a Finite Element solver and outsourced for several different structures. The effects of these changes were discussed in detail and conclusions regarding previous literature were drawn. Finally, the importance of a transient solution and the essentiality of the individual geometries, especially for further, more applied studies, became clearly visible.

References

[1] A Kovar-Panskus, P Louka, J-F Sini, E Savory, M Czech, A Abdelqari, PG Mestayer, and N Toy. Influence of geometry on the mean flow within urban street canyons–a comparison of wind tunnel experiments and numerical simulations. *Water, Air, & Soil Pollution: Focus*, 2(5):365–380, 2002.

[2] P Kastner-Klein, R Berkowicz, and R Britter. The influence of street architecture on flow and dispersion in street canyons. *Meteorology and Atmospheric Physics*, 87(1):121–131, 2004.

[3] Priyadarsini Rajagopalan and N Wong. Parametric studies on urban geometry, airflow and temperature. *International journal on architectural science*, 6(3):114–132, 2005.

[4] Jae-Jin Kim and Jong-Jin Baik. A numerical study of thermal effects on flow and pollutant dispersion in urban street canyons. *Journal of applied meteorology*, 38(9):1249–1261, 1999.

[5] Tim R Oke. Street design and urban canopy layer climate. *Energy and buildings*, 11(1): 103–113, 1988.

7 Appendix

A: Figures

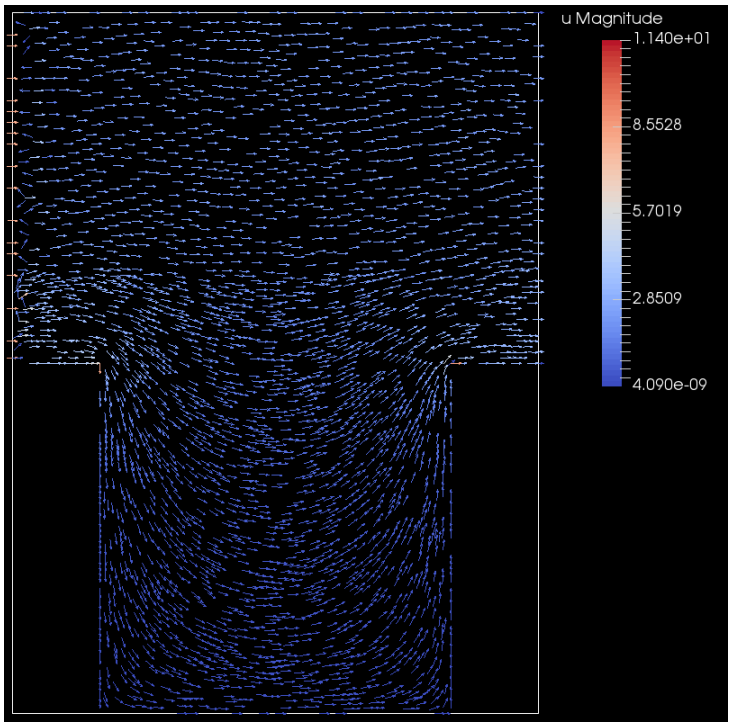

Figure 3: Vector field solution at time $t = 0.02[s]$ for $\frac{W}{H} = 1$

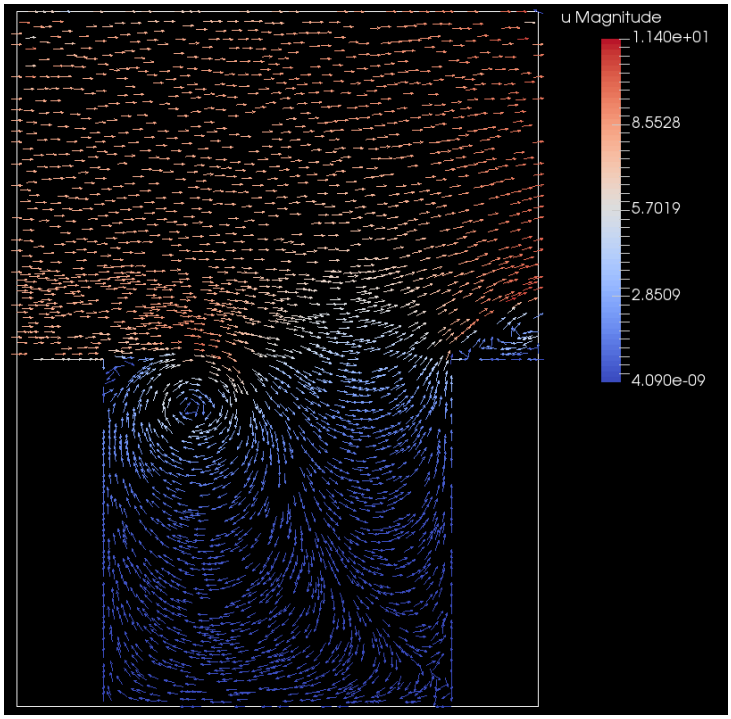

Figure 4: Vector field solution at time $t = 2.50[s]$ for $\frac{W}{H} = 1$

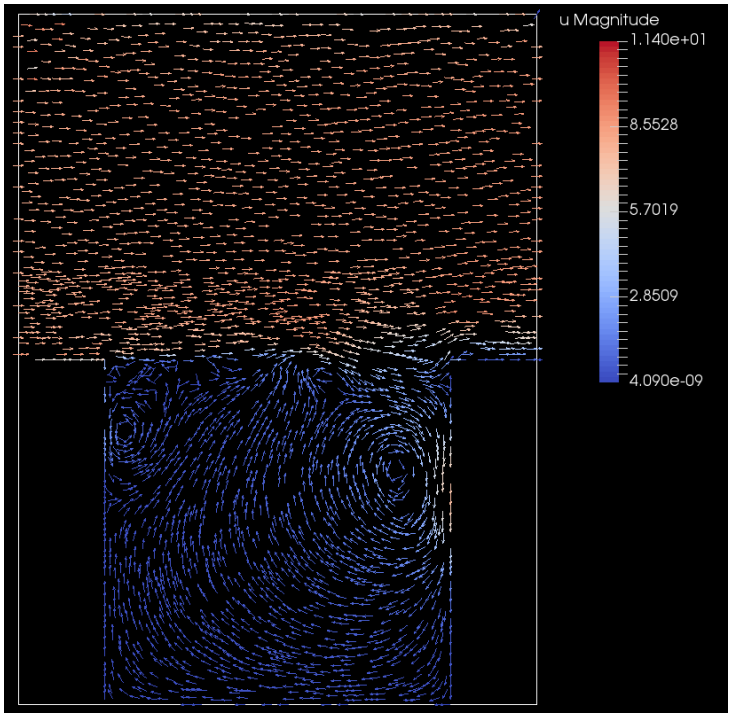

Figure 5: Vector field solution at time $t = 5.00[s]$ for $\frac{W}{H} = 1$

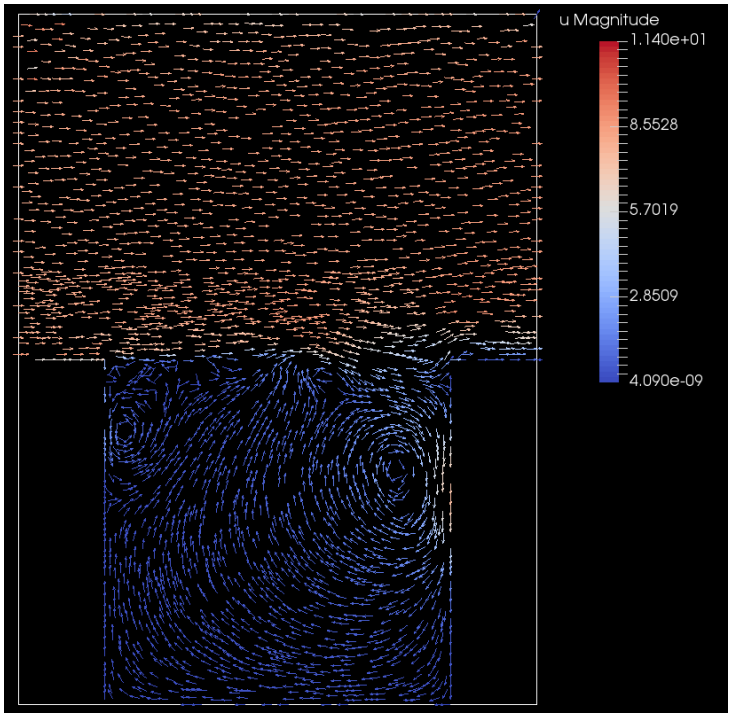

Figure 6: Vector field solution at time $t = 7.50[s]$ for $\frac{W}{H} = 1$

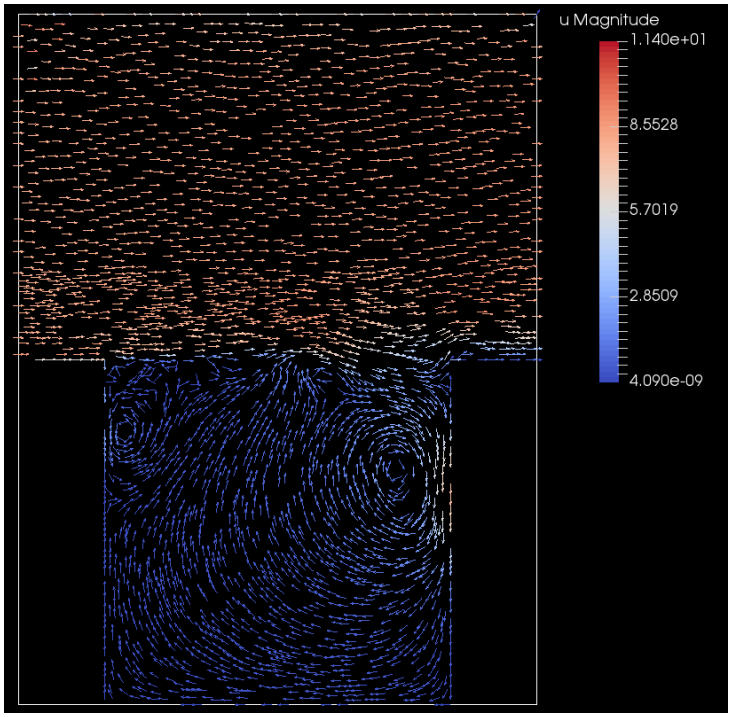

Figure 7: Vector field solution at time $t = 10.00[s]$ for $\frac{W}{H} = 1$

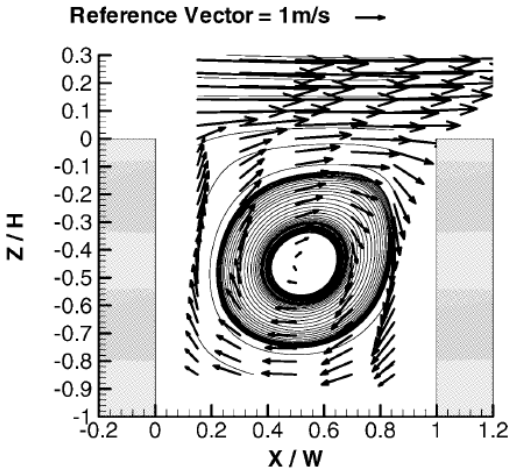

(a) Experimental result, from [4].

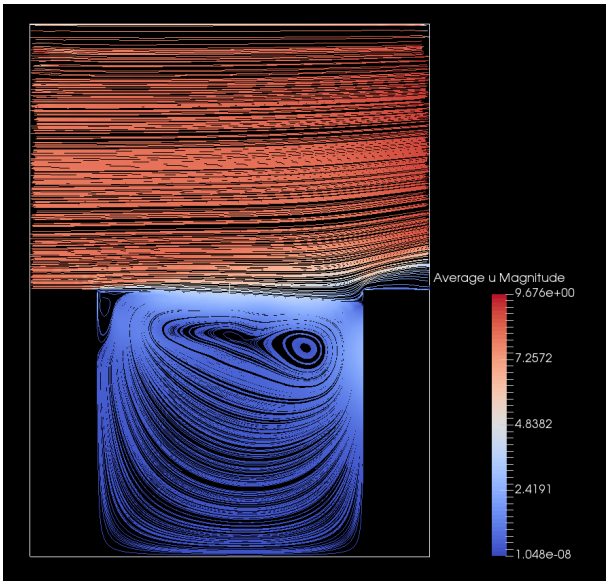

(b) Time averaged solution ($t = 1$ to $t = 10$).

Figure 8: Streamline validation with experimental results for $\frac{W}{H} = 1$.

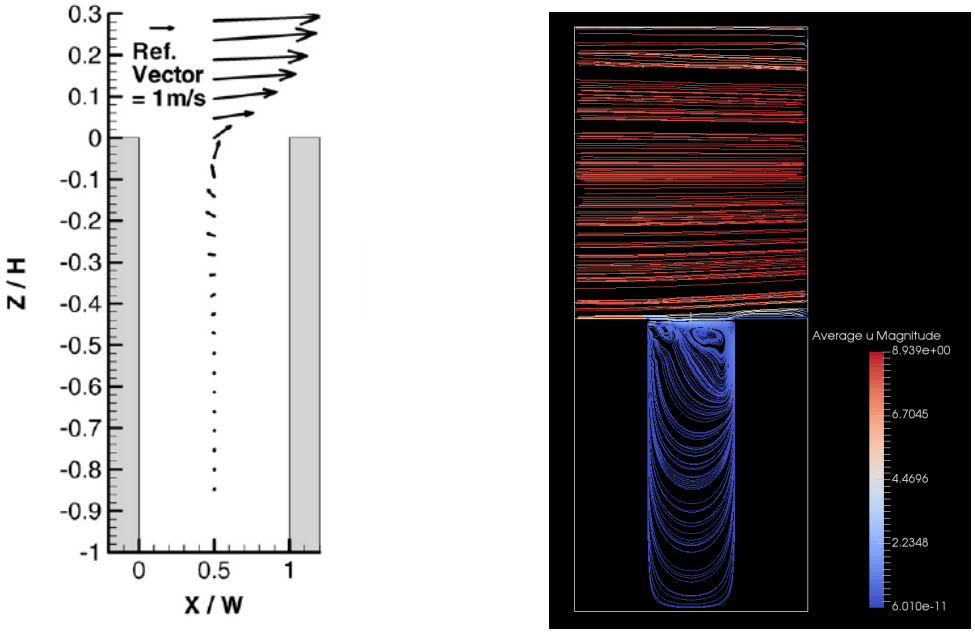

(a) Experimental result, from [4]. (b) Time averaged solution ($t = 1$ to $t = 10$).

Figure 9: Streamline validation with experimental results for $\frac{W}{H} = 0.3$.

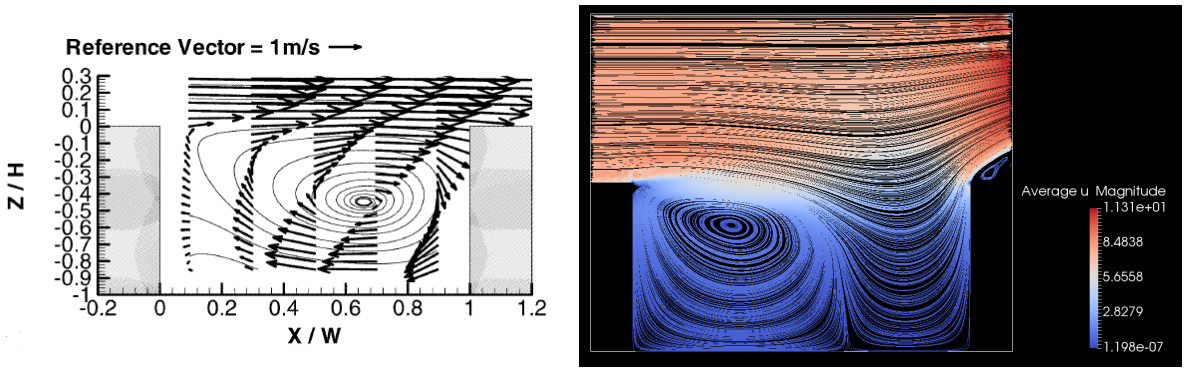

(a) Experimental result, from [4]. (b) Time averaged solution ($t = 1$ to $t = 10$).

Figure 10: Streamline validation with experimental results for $\frac{W}{H} = 2$.

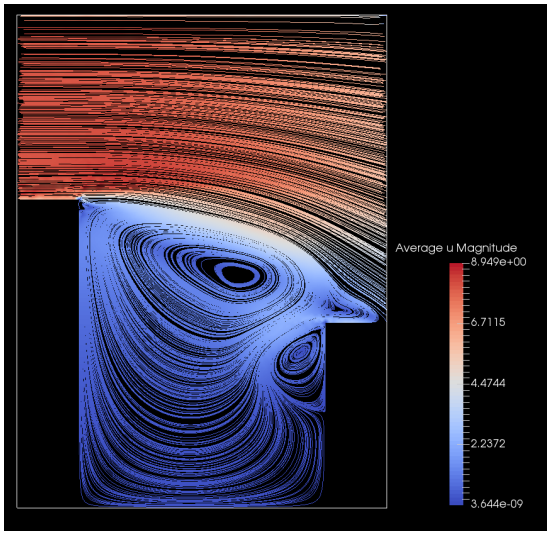

(a) $H_1 = 25[m]$ and $H_2 = 15[m]$

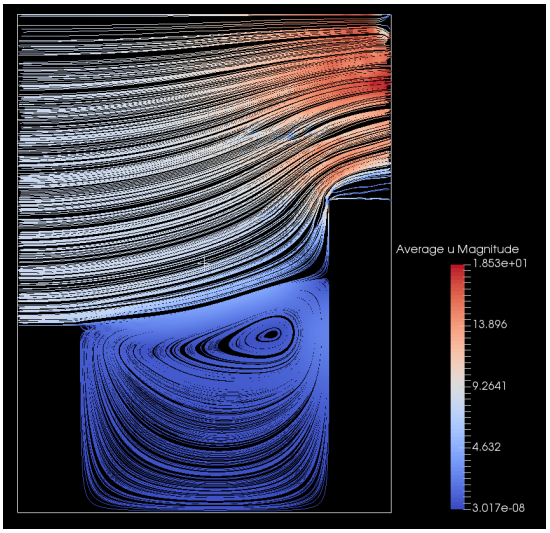

(b) $H_1 = 15[m]$ and $H_2 = 25[m]$

Figure 11: Streamlines for time averaged velocity ($t = 1$ to $t = 10$).

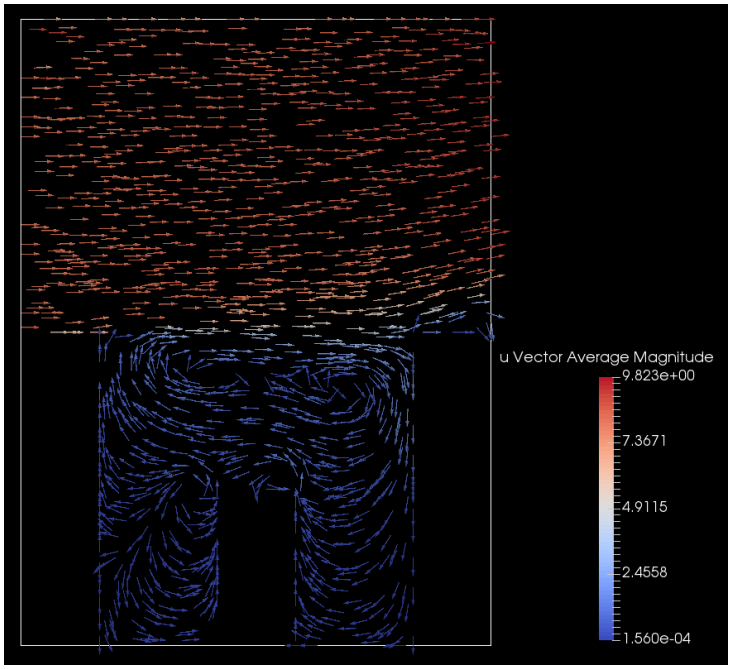

Figure 12: Time averaged velocity vector field ($t = 1$ to $t = 10$).

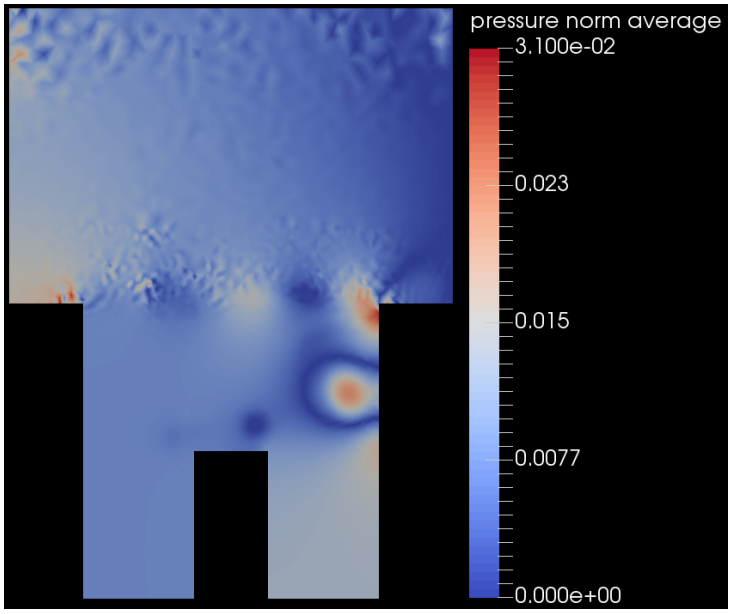

Figure 13: Time averaged pressure norm on domain with an additional obstacle

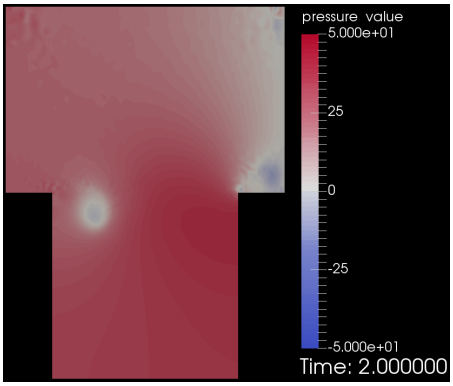

(a) $t = 2$

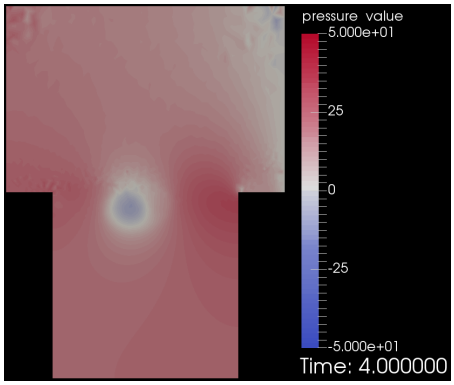

(b) $t = 4$

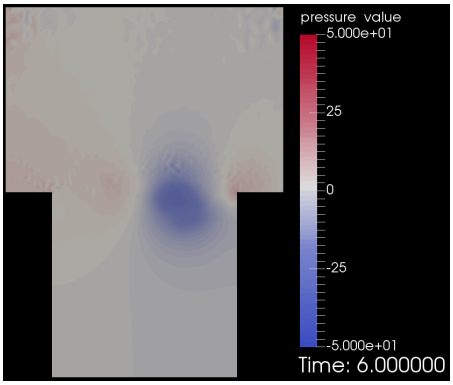

(c) $t = 6$

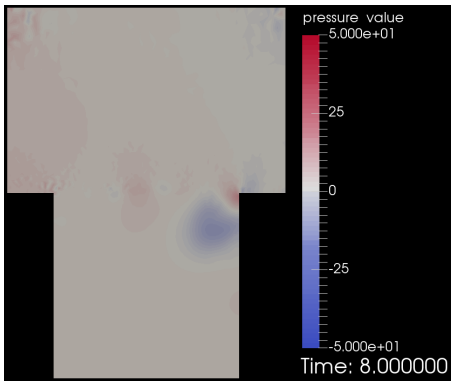

(d) $t = 8$

Figure 14: Pressure value at the change of time for the standard domain with $\frac{W}{H} = 1$

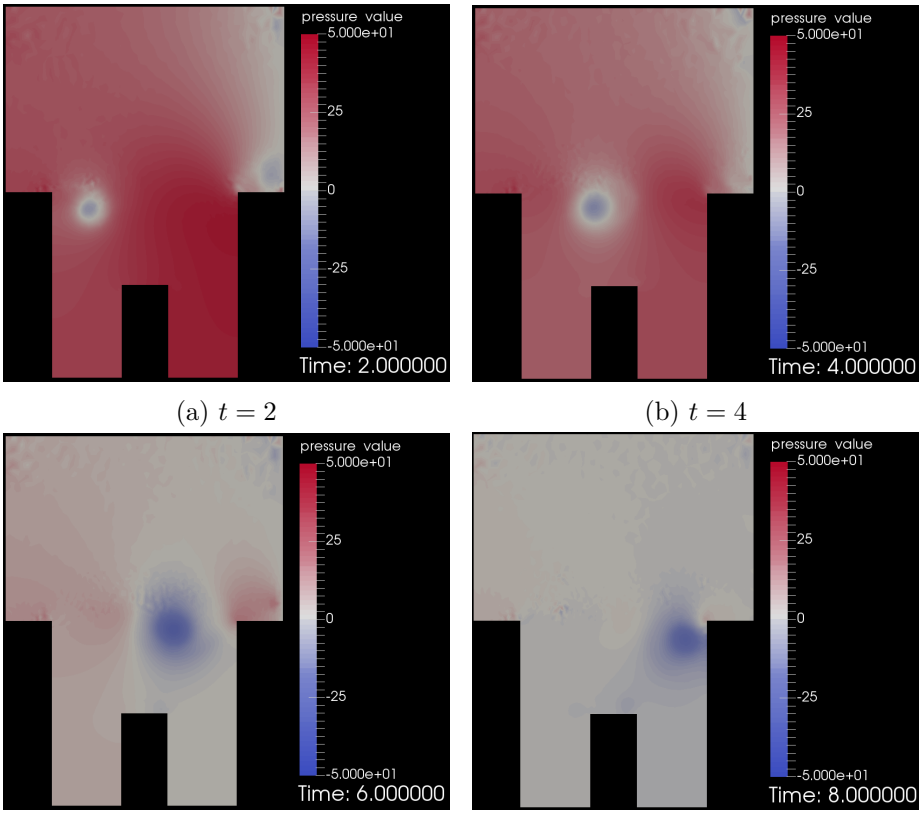

(a) $t = 2$ (b) $t = 4$

(c) $t = 6$ (d) $t = 8$

Figure 15: Pressure value at the change of time on domain with an additional obstacle

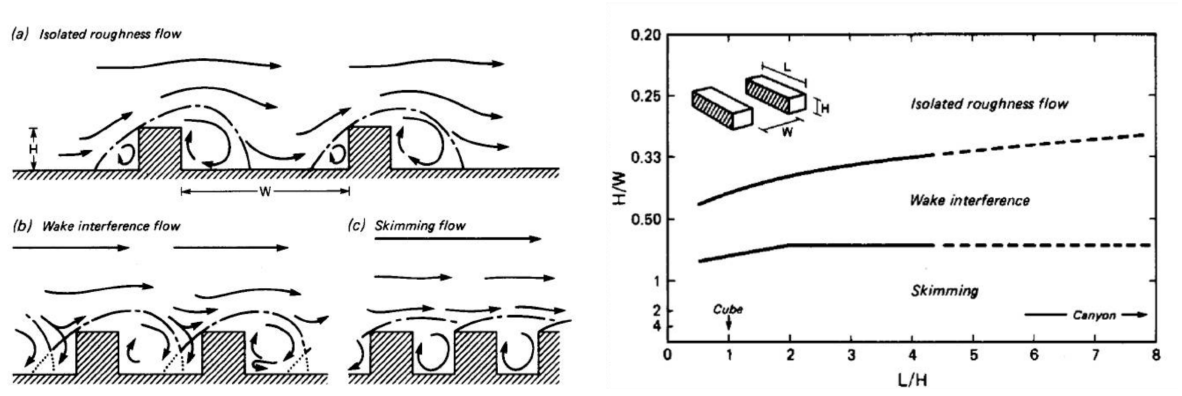

(a) Flow regimes associated with air flow over multiple buildings

(b) Threshold lines dividing the occurring flow into three regimes

Figure 16: Flow categorization dependent on width-height ratio, taken from [5]

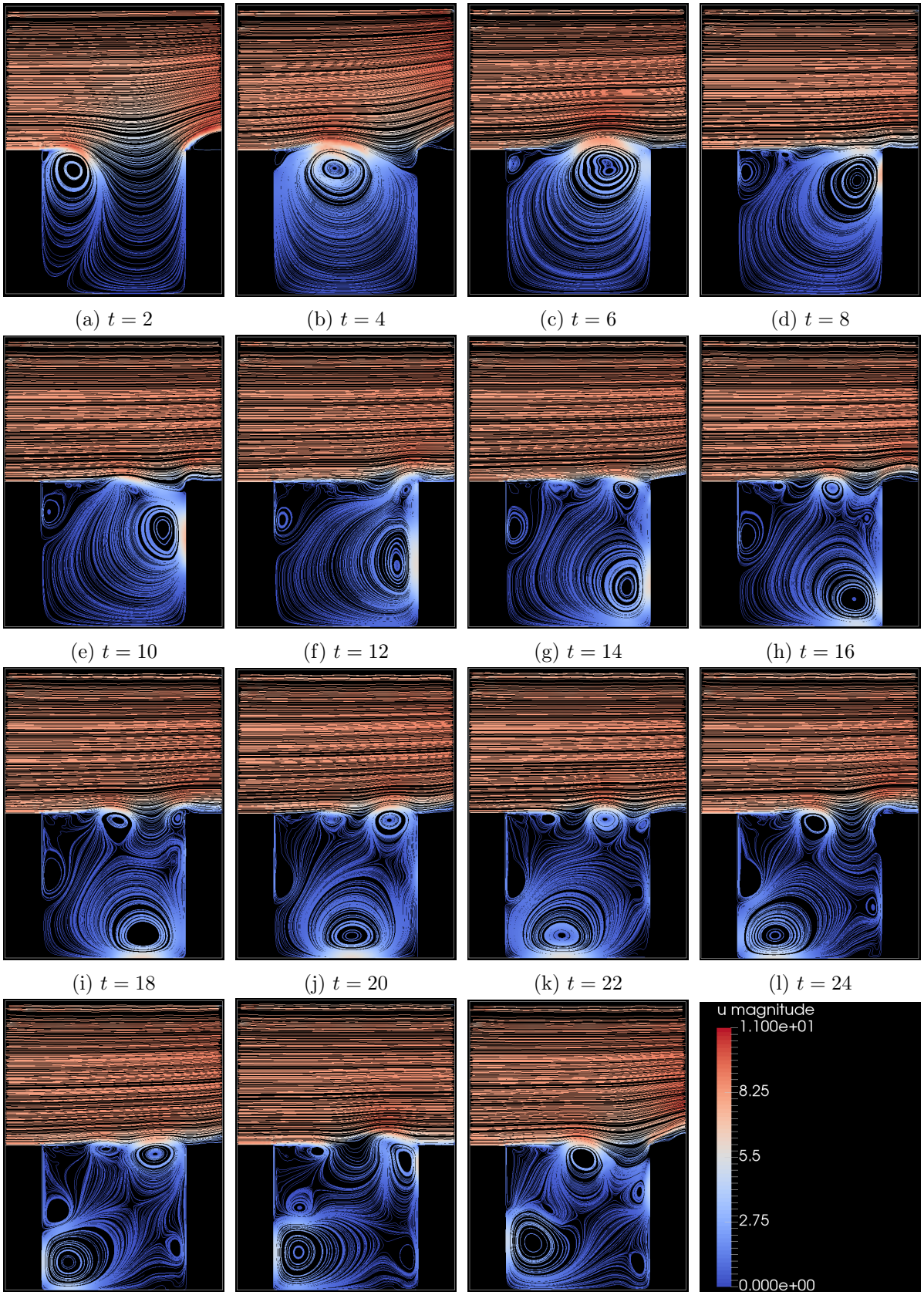

(a) $t = 2$ (b) $t = 4$ (c) $t = 6$ (d) $t = 8$

(e) $t = 10$ (f) $t = 12$ (g) $t = 14$ (h) $t = 16$

(i) $t = 18$ (j) $t = 20$ (k) $t = 22$ (l) $t = 24$

(m) $t = 26$ (n) $t = 28$ (o) $t = 30$ (p) colormap

Figure 17: Time dependent streamline plot with velocity magnitude for $\frac{W}{H} = 1$.

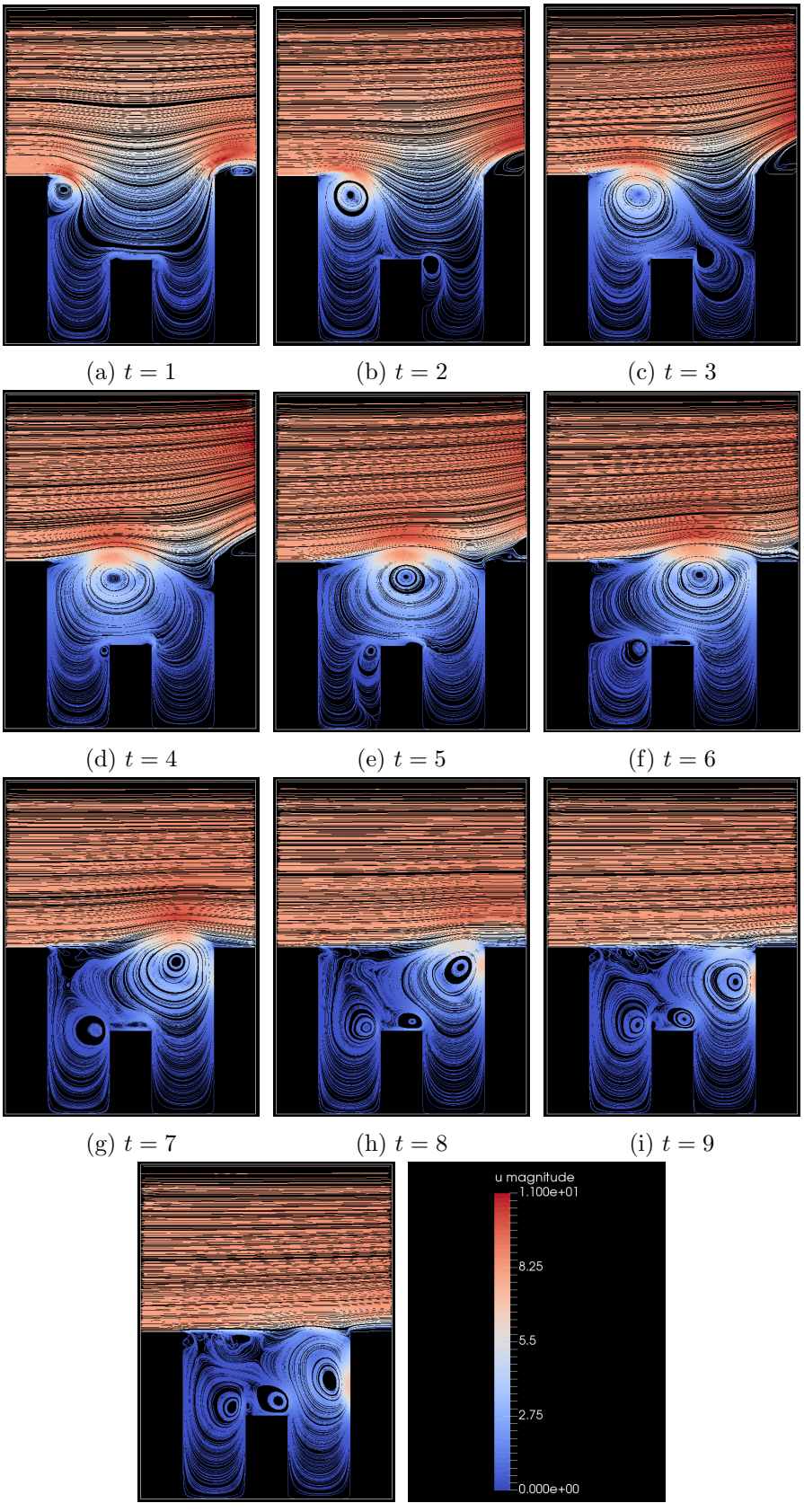

(a) $t = 1$ (b) $t = 2$ (c) $t = 3$

(d) $t = 4$ (e) $t = 5$ (f) $t = 6$

(g) $t = 7$ (h) $t = 8$ (i) $t = 9$

(j) $t = 10$ (k) colormap

Figure 18: Time dependent streamline plot with velocity magnitude for three buildings.